2012 LLNL Nuclear Forensics Summer Program

Glenn T. Seaborg Institute
Lawrence Livermore National Laboratory
Physical and Life Sciences
Livermore, CA 94550, USA

Director: Annie Kersting (kersting1@llnl.gov)
Education Coordinator: Nancy Hutcheon
Administrator: Camille Vandermeer
Website https://seaborg.llnl.gov/

Sponsors:
National Technical Nuclear Forensics Center, Domestic Nuclear Detection Office, Department of Homeland Security
LLNL: Glenn T. Seaborg Institute, Physical and Life Sciences Directorate

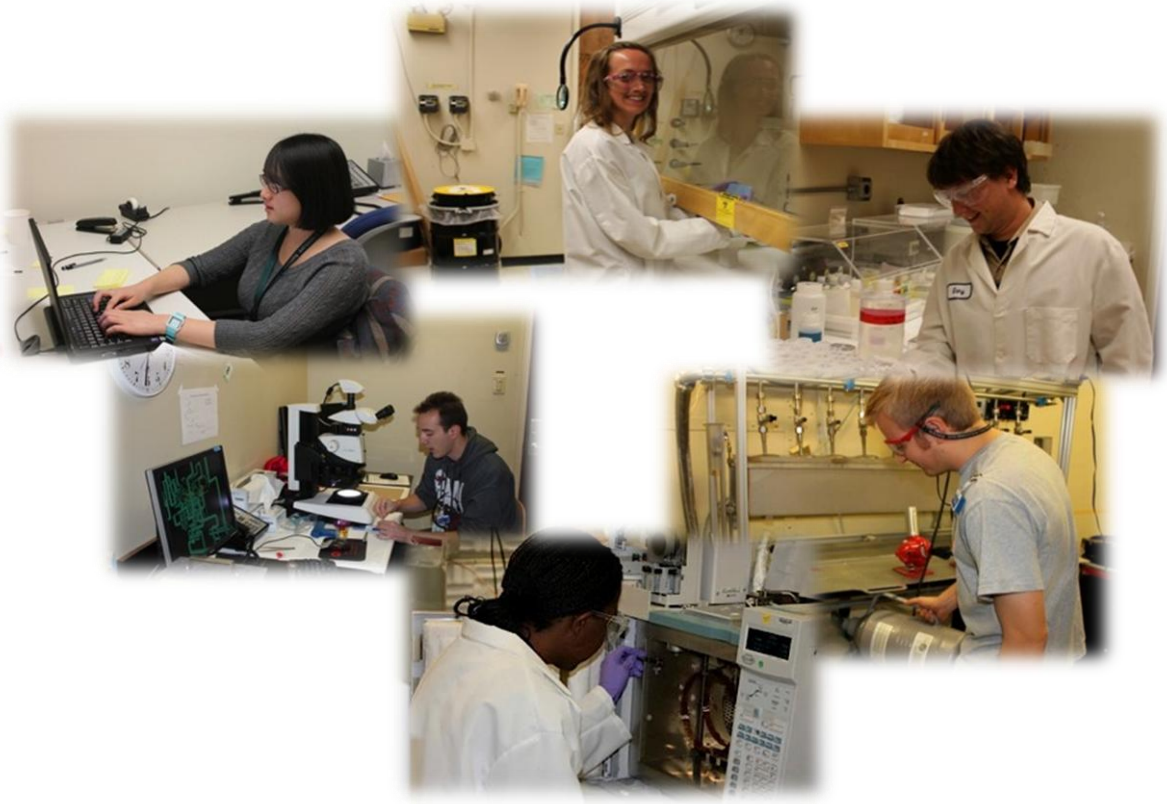

LLNL-TR-604174

The Lawrence Livermore National Laboratory (LLNL) Nuclear Forensics Summer Program is designed to give both undergraduate and graduate students an opportunity to come to LLNL for 8-10 weeks during the summer for a hands-on research experience. Students conduct research under the supervision of a staff scientist, attend a weekly lecture series, interact with other students, and present their work in poster format at the end of the program. Students also have the opportunity to participate in LLNL facility tours (e.g. National Ignition Facility, Center for Accelerator Mass-spectrometry) to gain a better understanding of the multi-disciplinary science that is on-going at LLNL.

Currently called the Nuclear Forensics Summer Program, this program began 12 years ago as the Actinide Sciences Summer Program. The program is run within the Glenn T. Seaborg Institute in the Physical and Life Sciences Directorate at LLNL. The goal of the Nuclear Forensics Summer Program is to facilitate the training of the next generation of nuclear scientists and engineers to solve critical national security problems in the field of nuclear forensics and have the student experience conducing research at the Lab. We select students who are majoring in physics, chemistry, geochemistry, mathematics, nuclear engineering, chemical engineering and environmental sciences. Students engage in research projects in the disciplines of actinide and radiochemistry, isotopic analysis, computational analysis, radiation detection, and nuclear engineering in order to strengthen the 'pipeline' for future scientific disciplines critical to DHS (DNDO), NNSA.

This is a competitive program with over 100 applicants for the 8-10 slots available. Students come highly recommended from universities all over the country. For example, this year we hosted students from Clemson University, Massachusetts Institute of Technology, University of Nevada, Las Vegas, University of Minnesota, University of Cincinnati, Duke University, Pennsylvania State University, University of Missouri and University of California, Berkeley. (See Table 1). We advertise with email to physics, engineering, geochemistry and chemistry departments throughout the U.S. We also host students for a day at LLNL who are participating in the D.O.E. sponsored "*Summer School in Radiochemistry"* course held at San Jose State University and have recruited from this program. We also participate in the Nuclear Forensics Undergraduate Summer Program sponsored by DHS-DNDO (FY12 held at University of Missouri) and recruit potential students.

This year students conducted research on such diverse topics as: actinide (Np, U, Pu) isotopic fingerprinting, statistical modeling in nuclear forensics, actinide analysis for nuclear forensics, environmental radiochemistry, radiation detector materials development, coincidence counting methods, nuclear chemistry, and heavy element separations chemistry.

In addition to hands on training, students attend a weekly lecture series on topics applicable to the field of nuclear forensics (see Table 2). Speakers are experts from both within and external to LLNL. Speakers are able to discuss the importance of their work in the context of advances in the field of nuclear forensics.

Graduate students are invited to return for a second year at their mentor's discretion. We encourage the continuation of research collaboration between graduate student, faculty advisor and laboratory scientists. Graduate and undergraduate students on fellowship such as the Nuclear Forensics Graduate Fellowship are invited into our summer program. This year we had three; two in the graduate program and one in the undergraduate program.

We use our summer program to create a successful pipeline of top quality students from universities across the U.S. Since 2002, 42 students have returned and/or conducted their graduate research at LLNL:

- 12 have become postdoctoral fellows,
- 2 have become postdoc positions at other national labs,
- 7 have been hired as career scientists at LLNL.
- 3 have hired at career scientists at other national labs, and
- 3 three are currently faculty in the area of nuclear forensics/radiochemistry.

A big factor in the success of this program is the dedication of the staff scientists who volunteer to mentor the summer students. In FY11, funding from the Nuclear Forensics Graduate Mentoring Program (sponsor: DNDO) helped to partially support the time staff took to teach the summer interns. Staff scientists we able to take the necessary time to develop an appropriate summer project, oversee the safety training and dedicate more time helping the interns maximize their productivity and scientific potential.

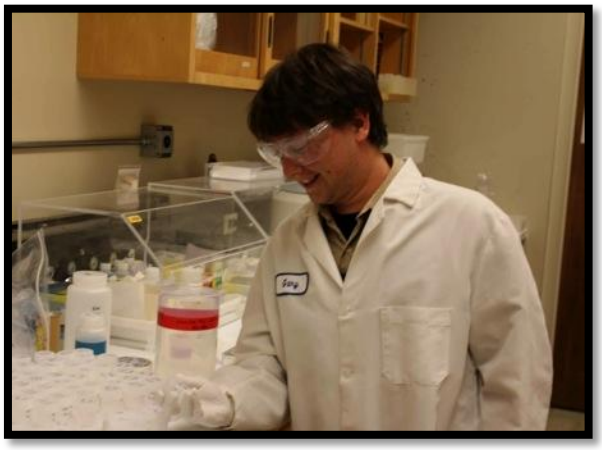

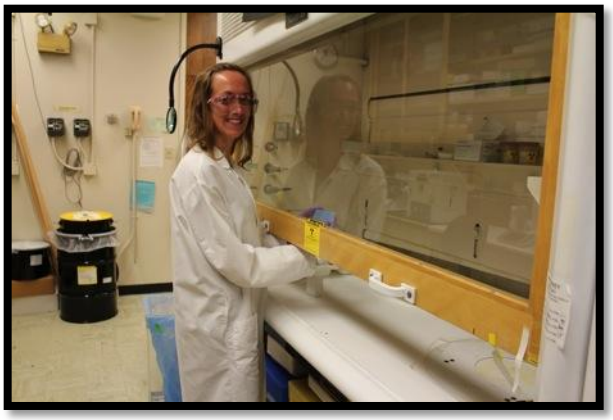

Table 1 Summer Students

No.	Student	Major	University	Year
1	Elizabeth DeRubeis	Geology	California State University, East Bay	Grad
2	John Despotopulos	Chemistry	University of Nevada, Las Vegas	Grad
3	Marc Fitzgerald***	Chemistry	University of Nevada, Las Vegas	Grad
4	April Gillens**	Environmental Engineering & Earth Sciences	Clemson	Grad
5	Mitchell Goshert	Chemistry	University of Missouri	Grad
6	Timothy Jacomb-Hood*	Nuclear Engineering	Pennsylvania State University	Undergrad
7	Erin Kenney	Mathematics	Massachusetts Institute of Technology	Undergrad
8	Anna Lindquist	Geophysics	University of Minnesota	Grad
9	Lisa Meyers	Nuclear Engineering	University of Cincinnati	Grad
10	Grayson Rich	Physics	Duke University	Grad
11	Barbara Wang**	Nuclear Engineering	University of California, Berkeley	Grad

* = Nuclear Forensics Undergraduate Intern
**= Nuclear Forensics Graduate Fellows
***= Has since became a Nuclear Forensics Graduate Fellow (9/12)

Table 2 Seminar Schedule

Date	Speaker	Topic
6/21/12	Dawn Shaughnessey Chemical Sciences Division, LLNL	Present Day Superheavy Element Discovery at LLNL and FLNR
6/28/12	Greg Spriggs, AX Division, LLNL	Fireball Physics – Nuclear Weapon Effects
7/2/12	Arthur Rodgers Atmospheric, Energy and Earth Division, LLNL	Prompt Forensics with Speed-of-Sound Data
7/12/12	Ben Jacobsen, LLNL Naomi Marks, LLNL Rich Gostic, LLNL	Post-doctoral Research in Nuclear Forensics at LLNL
7/19/12	Nick Scielzo Physics Division, LLNL	Beta-Delayed Neutron Spectroscopy Using Trapped Ions
7/27/12	Annie Kersting Seaborg Institute LLNL	Actinides in the Environment
8/1/12	Dr. Siegfried Hecker Stanford University	An eye on nuclear North Korea: Looking from the inside and the outside.

Table 3 Student Projects and Mentors

Student	Mentor	Project
Elizabeth DeRubeis	Brad Esser	Using Rn-222 to estimate groundwater inflow to Martis Creek
John Despotopulos	Dawn Shaughnessy	Extraction Chromatographic Studies of Flerovium (Element 114) and Element 115 Homologs
Marc Fitzgerald	Rich Gostic	Forensic Signatures in Trinity Fallout Beads
April Gillens**	Mike Singleton	Carbon Stable Isotope Signatures of TBP
Mitchell Goshert	Patrick Huang	First Principles Study of $AnO_2(NO_3)_2(H_2O_2)$ (An=U,Pu) VI to V Reduction Potential
Timothy Jacomb-Hood*	Gary Eppich	Unraveling Environmental Contributions to Fallout Formation
Erin Kenney	Martin Robel	Improved Geolocation of Uranium Ore Concentrate through Geochemical Insights
Anna Lindquist	Kim Knight	Frozen in Time: Crystallinity and Composition help to Constrain the Cooling Environment of Fallout
Lisa Meyers	Ross Williams	Nuclear Forensic Signatures in Uranium Bearing Materials
Grayson Rich	Kareem Kazkaz	Development of a Lithium-Glass Based Composite Neutron Detector for He-3 Replacement
Barbara Wang**	Nick Scielzo	Cosmogenic Activation in the Neutrinoless Double-beta Decay Experiment CUORE

* = Nuclear Forensics Undergraduate Intern
**= Nuclear Forensics Graduate Fellows

This work was performed under the auspices of the U.S. Department of Energy by Lawrence Livermore National Laboratory under Contract DE-AC52-07NA2734

Using Rn-222 to estimate groundwater inflow to Martis Creek

Elizabeth DeRubeis[1,3], Richard Bibby[2], Bradley Esser[2], and Jean Moran[1]

[1] California State University East Bay, [2] Lawrence Livermore National Laboratory,

[3] Lawrence Livermore National Laboratory Glenn T. Seaborg Institute

Abstract: The goal of this project is to find areas where groundwater is flowing into the streams in Martis Valley, located near Lake Tahoe, California, in order to determine the stream system's dependence upon groundwater. Using Rn-222, a daughter product of the U-238 (found in granitic rocks) decay series, it is possible to determine areas of groundwater inflow, since surface waters will be lower in radon activity than groundwater. As the population in the Lake Tahoe/Truckee region increases, there will be an increase in how much groundwater is pumped for human consumption, leaving less available for the stream system. While many of the downstream areas of Martis Creek have low radon activities, there are some areas of relatively high activity, which indicate possible groundwater inflow.

Introduction:

- **Martis Valley is located just north of Lake Tahoe, California**
- **This may be a large recharge area due to snowfall/snowmelt and the mountains surrounding the valley**
- **The geology of the area is granitic, metamorphic, volcanic, alluvial, and glacial deposition. Due to the large presence of granite, Rn-222 is present in the area from the decay of U-238**
- **Rn-222 is volatile, has a half life of 3.82 days, and can be used as a groundwater tracer, since it has higher activity levels in groundwater than in surface water**
- **Sediment in the streambed may also release Rn-222 into surface water**
- **With climate change, an increase in temperatures would cause shorter periods of precipitation, leading to an earlier snowmelt. Groundwater inflow would be even more critical for streams to maintain their flows, but as population increases in the region, more demand will be placed on groundwater for human consumption.**

S-35 samples were also taken to help determine ages of the water

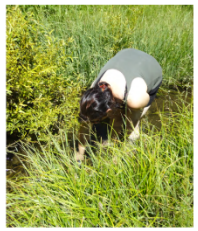

Samples were taken with no headspace, due to how volatile radon is

A map showing trails around Martis Creek. Sampling took place on the main branch of Martis Creek and along parts of Middle Martis Creek.

U-238 → Th-234 → Pa-234 → U-234 → Th-230 –> Ra-226 → **Rn-222** → Po-218 → Pb-214 → Bi-214 → Po-214 → Pb-210 → Bi-210 → Po-210 → Pb-206 (stable)

Rn-222 is a daughter product in the U-238 decay sequence. U-238 is commonly found in granitic rock

Methods:

In the field, water samples were collected in 20mL glass vials filled with 10mL of scintillation cocktail. Using a hooked syringe, 10mL of water was collected and injected beneath the cocktail, and the radon transferred from the water to the scintillation cocktail. The samples were then placed on a liquid scintillation counter to be analyzed for Rn-222 activity.

Results:

There was only one area that showed a significant amount of Rn-222 activity. This was from a stagnant pool of water that still had not gone dry three weeks after the initial sampling, though other sections of Middle Martis Creek had. There are several of these pools around the valley, which could be an indication that groundwater is flowing in.

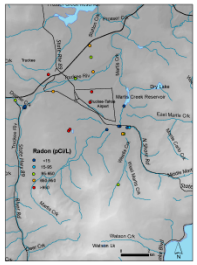

Both well and surface water show Rn activity, but wells have greater activity

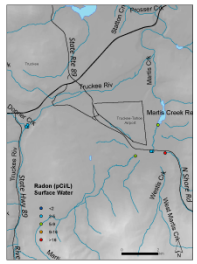

Surface water without groundwater inflow is low in Rn activity, generally below 10 pCi/L

Future Work:
1) Continued sampling for Rn-222 farther upstream in Martis Creek
2) Flow measurements along areas where samples are taken
3) Tracer study using SF6 and Xe, similar to one successfully performed at Alameda County Water District

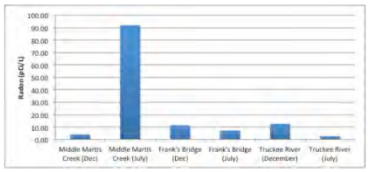

Comparisons between winter and summer radon activity in surface water show potential groundwater inflow areas.

Discussion:

The lack of Rn-222 activity in the stream could mean one of two things.
1) Groundwater has less of a role in the streams in Martis Valley than was previously thought, or 2) Groundwater is coming into the streams, but farther upstream, and is degassing before it reaches the areas that sampling took place in. It is likely the latter, as the pools of stagnant water have not gone dry, while other areas of the streams have become dry. Future sampling will occur in areas farther upstream to determine if this is the case.

References:
Cook, P.G., Lamontagne, S., Berhane, D. and Clark, J.F. (2006) "Quantifying groundwater discharge to Cockburn River, southeastern Australia, using dissolved gas tracers 222Rn and SF6.." Water Resources Research (42), W10411
Cox, C. and Esser, B.K. (2009) "Estimating groundwater inflow to Squaw Creek using Radon." LLNL Nuclear Science Intern Program
"Status and understanding of groundwater quality in the Tahoe-Martis, Central Sierra, and Southern Sierra study units, 2006-2007: California GAMA priority basin project" (2006) Scientific Investigations Report 2011-5216.

This work performed under the auspices of the U.S. Department of Energy by Lawrence Livermore National Laboratory under Contract DE-AC52-07NA27344.

LLNL-POST-569095

Extraction Chromatographic Studies of Flerovium (Element 114) and Element 115 Homologs

John Despotopulos[1], Narek Gharibyan[2], Julie Gostic[2], Roger Henderson[2], Ken Moody[2], Dawn Shaughnessy[2], Ralf Sudowe[1], Evgeny Tereshatov[2]

[1]University of Nevada – Las Vegas, [2]Chemical Sciences Division – Lawrence Livermore National Laboratory

INTRODUCTION AND MOTIVATION

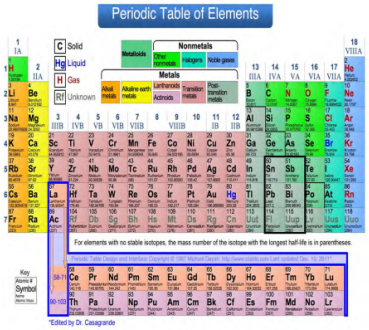

Recent studies of the chemical behavior of element 112 and 114 in the gas phase together with the discovery of isotopes with suitable half-lives have spurred a renewed interest in the development of suitable chemical systems to study the solution chemistry of elements with Z ≥ 114 [1,2]. Due to the short half-lives of the transactinide elements, fast and efficient separations are necessary so that the chemical properties of these elements can be compared to those of their lighter homologs. Separations based on extraction chromatography resins show promise for achieving the required short separation times, high yields and high separation factors that are required for transactinide studies. The adsorption of Pb and Sn, the lighter homologs of element 114, on Eichrom's Pb extraction chromatographic resin has been investigated from various acid matrices to evaluate its suitability for the study of element 114. Similarly, Bi and Sb, the lighter homologs of element 115, have been used to evaluate this resin for the investigation of element 115.

TRANSACTINIDE CHEMISTRY CHALLENGES

- Low production rates, with only a few atoms produced over the entire cycle.
- Short lifetimes, ranging from 10^{-9} seconds to a few hours.
- Chemical system must be reliable, robust, fast, and extremely efficient for ultra-trace applications (Automation required).

PROJECT GOALS

- Continue research aimed at the production of transactinide elements.
- Develop a chemical system for separating the homologs and pseudo-homologs of element 114 and 115 (Sn, Pb and Sb, Bi respectively).
- Separation scheme must give knowledge of the chemical form of the homologs and pseudo-homologs during the separation procedure, to allow extrapolation of the transactinide elements chemical properties.
- Chemical system must be automatable.

Physical and Life Sciences Directorate

CAMS ISOTOPE PRODUCTION

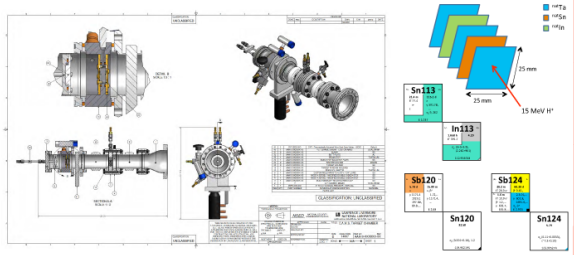

EICHROMS Pb RESIN AND BATCH STUDY PROCEDURE

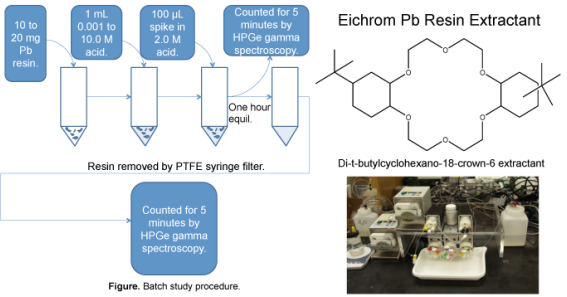

Figure. Batch study procedure.

RESULTS

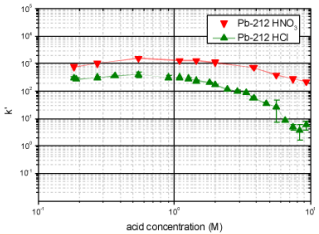

Figure. The batch uptake (k') of ^{212}Pb as a function of nitric acid and hydrochloric acid media on Pb resin (50-100 µm) with a 1 hour equilibration time.

ACKNOWLEDGEMENTS

This work was performed under the auspices of the U.S. Department of Energy by Lawrence Livermore National Laboratory under Contract DE-AC52-07NA27344. This work was funded by the Laboratory Directed Research and Development Program at LLNL under project tracking code 11-ERD-011. The authors would like to thank Jeff Rolfes for his help.

RESULTS Cont.

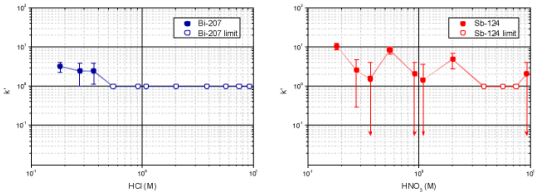

Figure. The batch uptake (k') of ^{207}Bi as a function of hydrochloric acid (left) and ^{124}Sb as a function of nitric acid (right) on Pb resin (50-100 µm) with a 1 hour equilibration time.

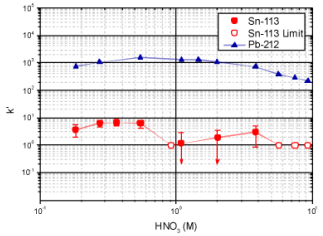

Figure. The batch uptake (k') of ^{212}Pb and ^{113}Sn as a function of nitric acid media on Pb resin (50-100 µm) with a 1 hour equilibration time.

CONCLUSIONS AND FUTURE WORK

Initial batch studies show a strong uptake of Pb by Eichrom's Pb resin from both hydrochloric and nitric acid matrices. Similar experiments indicate that Sn has a very low uptake by the Pb resin; thus a potential Pb/Sn separation scheme is possible. Both Bi and Sb show low uptakes by the Pb resin, indicating a new extractant or matrix must be explored for this separation. Future work will seek to establish: the best acid matrices and elution concentrations to perform Pb, Sn and Bi, Sb separations; determine the chemical form of the homologs during separation; and expand separation procedures to include the pseudo-homologs, Hg, Cd and Tl, In for element 114 and 115, respectively. The separation schemes will be evaluated, off-line and on-line, with short-lived homologs produced at the LLNL CAMS facility.

REFERENCES

[1] R. Eichler *et al.*, "Chemical characterization of element 112," Nature 447, 72-75 (2007).
[2] R. Eichler *et al.*, "Indication for a volatile element 114," Radiochim. Acta 98, 133-139 (2010).
[3] E. P. Horwitz, M. L. Dietz, S. Rhoads, C. Felinto, N. H. Gale, and J. Houghton, "A lead-selective extraction chromatographic resin and its application to the isolation of lead from geological samples," Analytical Chemica Acta 292, 263-273 (1994).

Forensic Signatures in Trinity Fallout Beads

Marc Fitzgerald[1], Richard Gostic, Greg Spriggs, Ian Hutcheon
[1]University of Nevada – Las Vegas

Glenn T. Seaborg Institute

UNLV UNIVERSITY OF NEVADA LAS VEGAS

Abstract

Analysis of fallout particles from Trinity and other nuclear explosions is central to understanding the fallout formation process. Insight into this process is important in order to quantify the environmental consequences of aboveground nuclear testing. Historical studies have investigated the average abundance and spatial distribution of radionuclides within fallout debris taken from near ground zero, but none have characterized the perturbation of the stable elements as a consequence of extreme heating. We show, through inductively coupled plasma mass spectrometry, that substantial variation exists in yttrium, ytterbium and thulium with respect to other rare earth elements (REE). This pattern is not completely explained by historical fallout models, and merits further investigation. (1) We also find an overabundance of copper, ruthenium, lead, and actinides in the fallout beads, which were likely derived from the testing environment of the explosion.

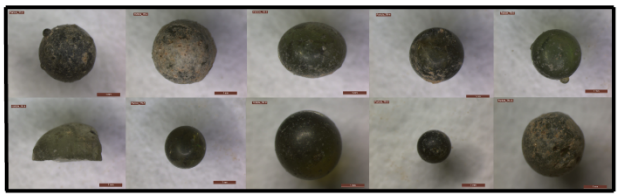

Figure 1: Trinity fallout beads used in the experiment

Experimental Objective and Design

- **Main Goal**: Characterization of the elemental composition of glassy fallout bead relative to the local soil.
- Ten fallout beads, pictured above, and one soil sample were characterized by nondestructive BeGE gamma spectroscopy[1] to estimate abundance of Am and Cs
- These results guided the dilution procedure used for subsequent inductively coupled mass spectrometry (ICP-MS)[2] analysis to survey major and trace element abundances
- One survey scanning 100 different isobars between masses 6 to 238 was performed. This was followed by a more detailed scan between masses 230 to 260, to focus specifically on the actinide masses.

Equations Used

(eq. 1) $$\%\,Dev = \frac{|r_{meas} - r_{true}|}{r_{true}} = \frac{\left|\left[\frac{x_n}{\sum_{n=1}^{i} x_n}\right]_{meas} - \left[\frac{x_n}{\sum_{n=1}^{i} x_n}\right]_{true}\right|}{\left[\frac{x_n}{\sum_{n=1}^{i} x_n}\right]_{true}} = \left|\frac{\left[\frac{x_n}{\sum_{n=1}^{i} x_n}\right]_{meas}}{\left[\frac{x_n}{\sum_{n=1}^{i} x_n}\right]_{true}} - 1\right|$$

1. The BeGe detector used in this experiment was a Canberra 38/30
2. The quadrupole ICP-MS used this experiment was an agilent 7500i

Results

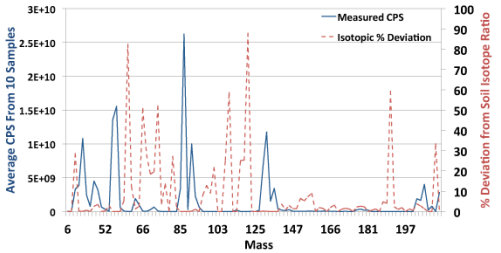

Figure 2: Mass spectrum and interference taken from an average of the 10 individual glassy bead analyses. Uncertainties in total signal are ~25%. The red dashed line, calculated from equation 1, shows the % deviation of the average fallout isotopic ratios from the ratios in soil. Large values suggest potential mass interferences.

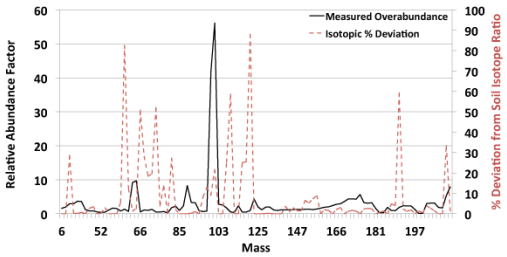

Figure 3: Average mass spectrum from the fallout beads normalized to the measured soil spectrum highlights mass excesses typical in the fallout. The red dotted line is as above.

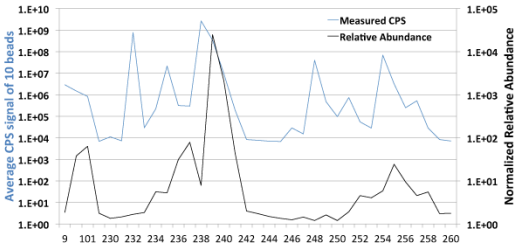

Figure 4: Average actinide mass spectrum and soil normalized spectrum focusing in the actinide mass region. Masses 237, 239, 240, and 241 show clear excess, likely due to Np and Pu. Respective oxides can be seen at masses 254, 255. Oxide formation for uranium was calculated at 2.6% from this signal. Signal at mass 9 and 100 are from a closer analysis of ^{99}Ru and ^{101}Ru.

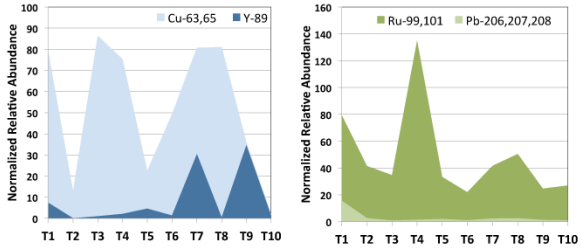

Figure 5,6: Variation in Cu, Y, Ru, and Pb relative to soil values by sample for each of 10 glassy fallout beads. Based on interference validation study (graphs at left), isobaric interferences are not observed at these masses, thus elemental abundances can be represented as the summed isotopic signals. Relative elemental abundances can vary between beads by more than a factor of 100.

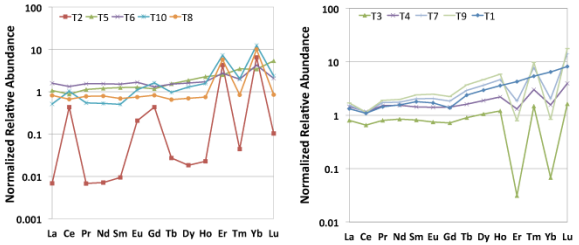

Figure 7,8: Relative lanthanide concentrations normalized to soil values show multiple patterns, similar to what is observed in Y (also a 3+ valence). Lanthanide masses 139-175 show minor potential mass interferences on the order of 3-4%, maximum.

Discussion and Future Work

Based on these analyses, we conclude that there is significant chemical excesses and substantial isotopic variation in the fallout beads relative to the local soil, as a result of mixing with the detonation debris. The elements copper, ruthenium, lead, as well as the actinides could only have been derived from the test. REE depletions observed in T2,T3,T8, and T10 relative to soil, in contrast with the other 6 beads (enriched in REE relative to soils) suggests variations in the fraction behavior prior to bead solidification. The lanthanide enriched samples yield a REE pattern consistent with the progression in melting point temperatures for the lanthanides. Samples T3, T4 ,T7, and T9 appear to have "sawtooth" depletion zones at cerium, gadolinium, erbium, and ytterbium. Corresponding zones of enrichment are observed in samples T2, T6, and T8 despite their overall depleted natures. This pattern suggests that, at least for cerium, gadolinium, and ytterbium, a change in chemistry such as oxidation must be occurring prior to fallout formation. Yttrium, which behaves similar to the lanthanides, also follows this "sawtooth" pattern for T7 and T9. Investigation using EXAFS/XANES techniques could reveal the chemical characteristics of the lanthanides and provide insight into fallout formation.

References

1.) Izrael, Yu. A. Radioactive Fallout After Nuclear Explosions and Accidents. *Radioactivity in The Environment*, **2002,** 3, 1-61
2.) Freiling, E. C. Radionuclide Fractionation in Bomb Debris. Science, **1961**, 133, 1991-1998

LLNL-POST-569172

This work was performed under the auspices of the U.S. Department of Energy by Lawrence Livermore National Laboratory under contract DE-AC52-07NA27344. Lawrence Livermore National Security, LLC

Development of a lithium-glass based composite neutron detector for ^{3}He replacement

Glenn T. Seaborg Institute

Grayson Rich, *Nuclear Forensics Internship Program*
Kareem Kazkaz, *Physics Division, PLS Directorate*

Motivated by the worldwide shortage of helium-3, we have fabricated a neutron detector based on a solid, composite material made of lithium-loaded scintillating glass cubes and scintillating acrylic, optimized both for neutron detection and gamma rejection. Monte Carlo simulations predict a 5" by 5" cylindrical detector of this type will have an intrinsic detection efficiency for unmoderated fission neutrons of 10%. A 2" diameter, 3" tall prototype, fabricated at LLNL this summer, is currently being experimentally characterized.

Physics of composite scintillator operation

Detectors are composed of grains of a scintillating material embedded throughout a supporting matrix.

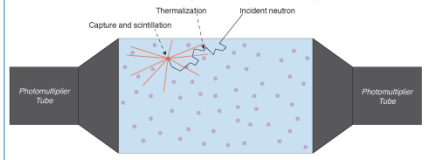

Neutrons incident on the detector thermalize in the acrylic and are then preferentially captured in the embedded, neutron-sensitive scintillator grains. The resulting scintillation light travels through the translucent matrix and is detected by photomultiplier tubes mounted to the volume.

Neutron capture events in the grains result in ions with stopping ranges on the order of 10 μm; consequently, such events deposit energy almost exclusively in the grains. By contrast, electrons from gamma-ray events have ranges on the order of millimeters in the grains and centimeters in the plastic; consequently, gamma-ray events are highly likely to deposit an appreciable amount of energy in the plastic matrix and can often be multi-site, multi-material events.

Through the use of pulse shape discrimination (PSD), the different timing characteristics of scintillation light from the grains and the plastic allow for determination of the material(s) in which the energy deposition took place, allowing rejection of gamma-ray events with minimal reduction of accepted neutron events.

Areas for improvement over earlier efforts

Several groups have recently explored composite detectors featuring lithium gadolinium borate (LGB) as the embedded scintillator and it was found that only captures on ^{6}Li were reliably separable from gamma-ray contamination. In the PSD plot shown below, obtained with an LGB detector, the island centered around 2.5 MeVee is attributed to captures on ^{6}Li, while the island at about 0.8 MeVee corresponds to ^{10}B captures (from [Nel11]).This motivates the selection of an alternative embedded scintillator without isotopes with competitive neutron capture cross sections.

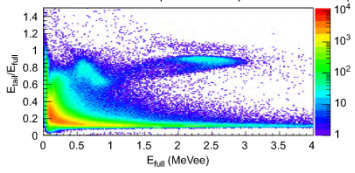

Numerous candidate embedded scintillator materials were considered, subject to criteria aimed at optimizing ^{6}Li capture efficiency and collection of the resulting scintillation light in addition to maintaining high gamma-rejection capabilities. KG2-type lithium glass was chosen for its high number of lithium nuclei per mole, its desirable scintillation time constant, and its closely matched index of refraction with the PVT matrix.

Following selection of a scintillator material, its dimensions can be optimized to maximize energy deposition by the ions resulting from a neutron capture reaction. Following simulations to determine the mean penetration depth before capture of neutrons incident on lithium glass, we utilized a 1-D analytical model developed by Kazkaz *et al.* to determine an optimal grain dimension of 1.5 mm [Kaz11].

Simulations of Li-glass composite detectors

- Monte Carlo simulations using GEANT4 were conducted to determine efficiency for detection of unmoderated fission neturons from ^{252}Cf and to estimate sensitivity to gamma rays.
- The neutron peak region of interest (NPR) was defined by a ±3σ window of a Gaussian fit to the peak in energy deposition in the cubes occurring at around 1.6 MeVee corresponding to captures on ^{6}Li in the glass (shaded in the plot below) [Fir61].
- In the ^{252}Cf source simulation illustrated in the upper plot, the isotropic source was located 16.2 cm from the circular face of the detector, generating 10M primary events. Counts inside the NPR were considered detected neutrons.
- For the monoenergetic gamma-ray sources, with 1M primary events directed towards the center of the circular face of the detector, counts inside the NPR represent potential contamination of the neutron counts by gamma-ray backgrounds.
- Our simulations *do* ***not*** consider the impact of PSD on gamma-ray backgrounds, which has been shown previously to reduce sensitivity to gamma backgrounds to the part-per-billion level for LGB detectors [Kaz11].

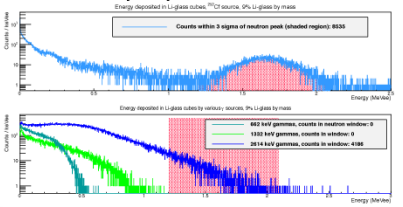

The results of extensive Monte Carlo simulations of our detectors predict an intrinsic detection efficiency for unmoderated fission neutrons from ^{252}Cf of 1% for the 2" diameter, 3" tall detector and 10% for the 5" by 5" detector.

Fabrication of prototype detectors

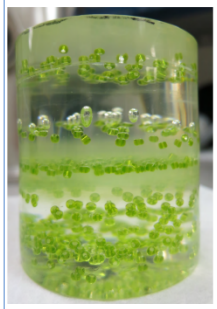

Initial tests of fabrication procedures were carried out using inexpensive glass beads of a similar dimension to our final cubes and PVT without scintillating dye. The photo at left shows the results of some early tests, with different layers clearly visible. Each layer was cured for different times and at different temperatures to determine ideal curing parameters. Several methods of mitigating bubble formation were also explored.

The images on the right are of the 2" x 3" prototype composed of lithium-glass cubes and dye-loaded PVT; both photos look along the length of the detector. The top image demonstrates the transmission of California sunshine through the volume while the bottom image shows fluorescence under UV excitation.

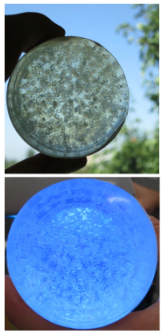

Compared to commercially available LGB-based detectors our prototype has much improved optical quality and a more even distribution of scintillator grains along its length.

Pulse shape analysis

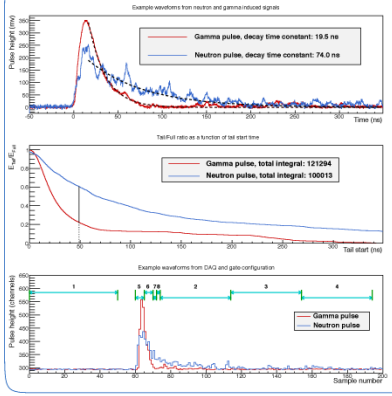

Pulses in the new composite detector, show distinguishable decay characteristics (upper plot) of two example waveforms acquired using the 2" x 3" prototype with a 5 GS/s oscilloscope.

Our data acquisition system utilizes a 200 MS/s digitizer with customized firmware that facilitates pulse shape analysis via 8 individually defined regions of integration. Different configurations and combinations of these gates facilitates effective and flexible PSD.

Adopting a tail start time of 49 ns was selected to maximize the separation of the E_{tail}/E_{full} ratios for the pulses shown at top (center plot).

The lower plot shows examples of both neutron- and gamma-induced events as captured by the digitizer. Overlaid on the traces are the integration gates selected to afford flexibility in analysis through making available several different tail start times.

Preliminary results

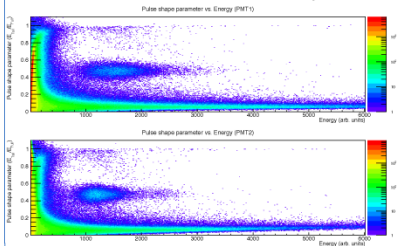

- *Preliminary PSD plots ^{252}Cf fission source 2" x 3" detector*
- *Neutron event island visible around PS parameter 0.5 and energy 1750*
- *Further optimization of analysis and PSA techniques could better distinguish neutron events*
- *This suggests ~10% intrinsic detection efficiency*

Bibliography and acknowledgements

- [Fir61] F.W.K. Firk and G.G. Slaughter. *An Improved Li6-loaded Glass Scintillator for Neutron Detection.* Nucl. Instrum. Methods, 13 (1961) 313-316.
- [Kaz11] K. Kazkaz, N.S. Bowden, and M. Pedretti. *Comparison of Lithium Gadolinium Borate Crystal Shards in Scintillating and Nonscintillating Plastic Matrices.* arXiv/nucl-ex, 1109 (2011).
- [Nel11] P. Nelson and N.S. Bowden. *Investigation of large LGB detectors for antineutrino detection.* Nucl. Instrum. Methods A, 660 (2011) 77-82.

The authors would like to acknowledge extreme gratitude for the assistance offered by Peter Thelin, H. Paul Martinez, Michelle A. Faust, and Lindsey K. Haselhorst, all of whom have a refreshing generosity, kindness, and dedication to science without which this project could not have proceeded.

This work performed under the auspices of the U.S. Department of Energy by Lawrence Livermore National Laboratory under Contract DE-AC52-07NA27344. LLNL-POST-571492

Lawrence Livermore National Laboratory

IM # 637732

Carbon stable isotope signatures of TBP

CLEMSON UNIVERSITY

April R. Gillens[1], Michael Singleton[2], and Brian A. Powell[1]; [1]Environmental Engineering and Earth Sciences, Clemson University, Clemson, SC
[2]Environmental Radiochemistry Group, Chemical Sciences Division, Physical and Life Sciences Directorate, Lawrence Livermore National Laboratory, Livermore, CA

Abstract

Tri-n-butyl phosphate (TBP) is the primary complexant of the Plutionium Uranium Reduction Extraction (PUREX) process. Its degradation products are dibutyl phosphate (DBP), monobutyl phosphate (MBP), butanol, and phosphoric acid. Many have agreed that in the case of phosphate esters such as TBP, acid hydrolysis will cleave the C-O bond whereas alkaline hydrolysis will attack the P-O bond[1]. The examination of carbon stable isotopes of TBP under reprocessing-like conditions may determine if TBP has a unique signature in nuclear reprocessing. This work aims to determine whether there is a carbon stable isotope fractionation of TBP as it is subjected to high acid and basic conditions. Further work will involve characterizing TBP degradation under the same conditions as this study using a developed FTIR-ATR technique[2] for the estimation of the amount of DBP produced in these reactions.

Experimental

Five milliliters of pure TBP (EMD Chemical, Inc.) was reacted with 5 ml of 50% wt NaOH in a 40 ml bottle. Another 5 ml of TBP was reacted with 5 ml of 8M HNO_3 (Fisher Scientific). The organic and aqueous phases were continuously agitated using a stir bar. Samples were taken in variable time increments. The last samples were analyzed using GC-FID (Agilent 6890) to determine the concentration of TBP remaining and the amount of degradation products produced. All samples were evaluated using GCC-IRMS for carbon stable isotope analysis. TBP and DBP standards were also analyzed on the EA-IRMS.

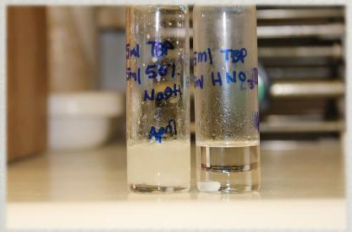

Figure 1. Acid and basic hydrolysis of TBP. TBP with 19M NaOH and TBP with 8M HNO_3 (left to right).

Results

The basic reaction was terminated after 4 days due to a crystal formation in the organic phase (Figure 1). Another basic reaction was reproduced but no stir bar was added for agitation. There was no crystal formation after six days in this reaction. The acidic reaction continued without issue until termination on day 6 (Figure 1). Based on the measured and calculated concentrations of TBP, it was determined that 81.9% of TBP was recovered in the acidic sample after 6 days in reaction with 8M HNO3 and that 80.9% of TBP was recovered in the basic sample after only 2 days in reaction with 19 M NaOH.

Table 1. Carbon stable isotope ($\delta^{13}C$) data of TBP in acid and basic reactions

Time (hr)	TBP/8M HNO3	TBP/19 M NaOH-1	Time (hr)	TBP/19M NaOH-2
0	-30.80	-30.80	0	-30.80
2	-30.28	-30.35	0.13	-30.80
25	-30.64	-30.46	28	-30.35
47	-30.72	-30.80	56	-30.39
98	-30.57			
149	-30.50			

Table 2. $\delta^{13}C$ of pure TBP & DBP

TBP	-30.80
DBP	-27.30

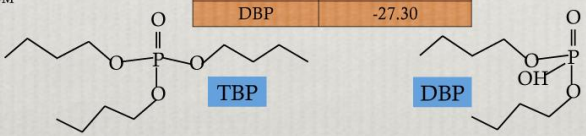

Discussion

Based on the current study, there was no determination of degradation products produced in the acid and basic reactions with TBP due to the lack of availability of diazomethane, which is a derivatizing agent for TBP. The DBP and MBP degradation products of TBP cannot be properly accounted for unless they are methylated with diazomethane. This study attempted to quantify the amount of DBP generated in sample by methylating the last sample drawn from the reaction, however, the last sample from the first basic hydrolysis reaction was depleted of TBP and known degradation products and last samples from the second basic hydrolysis and the acidic hydrolysis had not produced DBP at the time of final sampling. Although there is an estimated 20% loss of TBP in both acid and basic reaction and it is expected that degradation products did form in the sample, we cannot verify the amount of degradation products in these samples. Thus further work will be performed to quantify TBP degradation in acidic and basic solutions. However, the importance of this study is carbon stable isotopes of TBP and regardless of the amount of degradation products present in the TBP sample, the carbon stable isotope signatures of TBP did not undergo a measurable change as TBP was subjected to high acidic and basic concentrations which demonstrates the robust nature of the molecule. Hence, the need to further explore TBP degradation in a diluent system which is more practical considering TBP is diluted in the PUREX process.

Future Works

As aforementioned, a FTIR-ATR technique was developed for the rapid quantification of TBP and its degradation products (only DBP and MBP). Future work will attempt to couple the stable isotope data with this technique to characterize the degradation of TBP by acid and basic hydrolysis. The technique was developed based on the vibrational modes of TBP and DBP. Spectra of TBP sampled from an acid and basic reaction will determine where bonds are being cleaved on the TBP molecule.

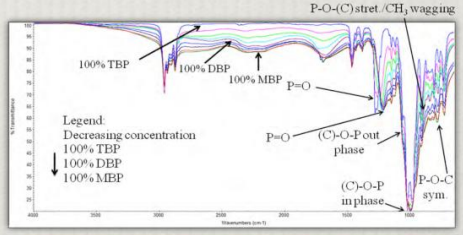

Chemical Species	Ratio	Position region cm^{-1}	Slope	Intercept	R^2
DBP/TBP	1		0.000117	0.0111	0.99
	2		4.99E-05	0.0136	0.95
	3		0.000863	1.3336	0.93
		770-785	0.063638	772.26	0.96
		1220-1235	0.125352	1206.3	0.96
DBP/MBP	1		-7.1E-06	0.0231	0.24
	2		-2.9E-05	0.0212	0.98
	3		-0.00262	1.7072	0.94
		770-785	-0.06943	784.41	0.92
		1220-1235	-0.15814	1235.6	0.97

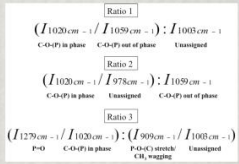

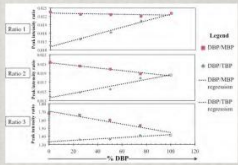

Acknowledgements

This research was performed under the Nuclear Forensics Graduate Fellowship Program, which is sponsored by the U.S. Department of Homeland Security, Domestic Nuclear Detection Office and the U.S. Department of Defense, Defense Threat Reduction Agency. This work performed under the auspices of the U.S. Department of Energy by Lawrence Livermore National Laboratory under Contract DE-AC52-07NA27344.

References

[1]W. W. Schulz and J. D. Navratil, The Science and Technology of Tributyl Phosphate, Vol. 1 CRC Press, Boca Raton, FL (1984).

[2]A. R. Gillens and B. A. Powell, Rapid Quantification of TBP and TBP Degradation Product Ratios by FTIR-ATR, J. Radioanaly and Nuc. Chem. (MARC IX Conference Proceedings), Accepted, Aug 2012.

Unraveling Environmental Contributions to Fallout Formation

Timothy Jacomb-Hood[1], Gary Eppich[2], Kim Knight[2], Gregory Spriggs[2], Richard Gostic[2], Michael Kristo[2], and Ian Hutcheon[2]

[1]The Pennsylvania State University [2]Lawrence Livermore National Lab

Overview

Following a near surface nuclear detonation, fallout is formed containing a mixture of the device, radioactivity released by the explosion, and the near ground zero environment. The precise mechanisms of fallout formation remain poorly understood. The current model of fallout formation is that the nuclear explosion evaporates the surrounding material, including the device. This material forms glasses that trap elements from the detonation and surrounding environment. Mixing and fractionation behavior may be a function of the different saturated vapor pressures at a given temperature and pressure [1].

For this study, we examined nine surface soil samples and six glassy fallout beads from the National Nuclear Security Site (NNSS). We measured major and trace element composition, mineralogy, U and Th concentration and isotopic composition of the soils, and U and Th concentration and isotopic composition of the glassy beads. We compare the isotopic information from the soils to that of the fallout glass in the context of chemical and mineralogical composition of NNSS soils. Soil samples were selected to be representative of three areas within the test site, and were believed to be minimally contaminated by historical testing.

Method

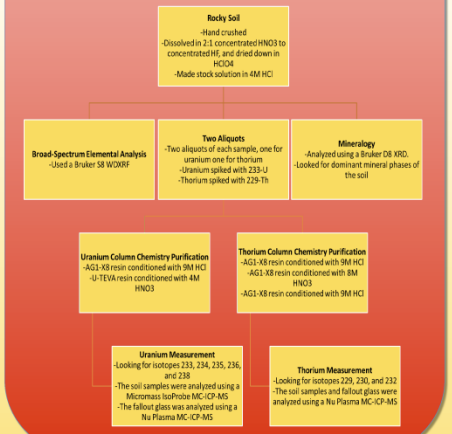

References

[1] Yu. A. Izrael, *Radioactive Fallout after Nuclear Explosions and Accidents* Oxford, UK: Elsevier, 2002

Soil Mineralogy and Elemental Composition

Three soils from three different NNSS locations were analyzed (n = 9). Soils from the same location generally show similar mineralogy and major element chemistry. Buckboard Mesa samples are dominated by silicates, while Frenchman Flat soils contained ~20% carbonates. North Yucca Flat samples show more variation between samples, and contain significant amounts of both carbonates and silicates.

Sample ID	Location	Comments	Mineralogy
NTS 86	Buckboard Mesa	Rocky, vegative	Quartz, Orthoclase, Sanidine
NTs 90		Rock sample	Quartz, Orthoclase, Sanidine
NTS 92		Loose rocky	Quartz, Orthoclase, Sanidine
NTS 127	Northern Yucca Flat	Rocky, loose	Quartz, Calcite, Dolomite
NTS 132		Loose soil	Calcite, Dolomite, Ankerite
NTS 134		Very rocky	Calcite Magnesian, Dolomite, Ankerite
NTS 137	Frenchman Flat	Playa	Quartz, Calcite Magnesian, Dolomite
NTS 139		Playa	Quartz, Calcite Magnesian, Dolomite
NTS 141		Loose dirt	Quartz, Calcite Magnesian, Dolomite

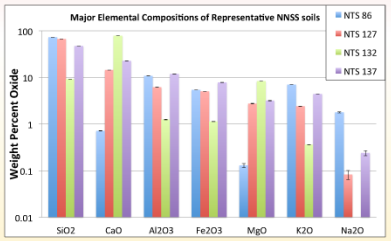

Major elements found in representative NNSS soils, measured by X-ray fluorescence. Large variations in the major element composition of the soils are apparent, suggesting that NNSS surface soils are both chemically and mineralogically heterogeneous.

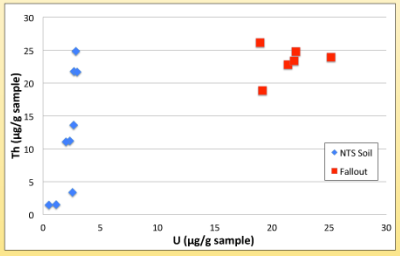

U and Th concentrations were measured by isotope dilution. Uranium concentrations vary by <5 µg/g, while Th concentrations are more scattered. The U and Th concentrations of the glass beads are a mixture of environmental and device contributions. 'Contaminated' soil samples NTS 86 and NTS 132, with elevated $^{235}U/^{238}U$ relative to natural, show similar U concentrations to the rest of the soil samples. Error bars are smaller than symbols.

Isotopic Composition

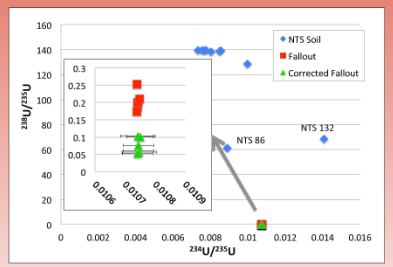

Glass bead $^{234}U/^{235}U$ is similar, in contrast with the soils, which display much larger variations. After correcting for soil U, $^{238}U/^{235}U$ of the glassy beads is lower by a factor of 3 than uncorrected values. Using an average U concentration from the soils of 2.26 µg and assuming an equal mass contribution, we show a simple subtraction to correct U isotopic compositions in the fallout for the environmental contribution (green data). This results in fallout glass enrichments of approximately 92% ^{235}U.

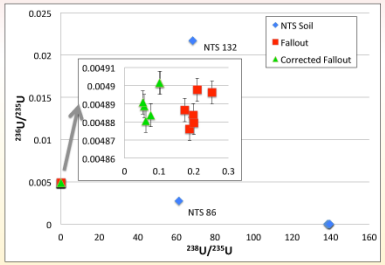

Most analyzed soils show natural uranium isotope compositions, with two exceptions. Soil sample NTS 86 falls between the fallout values and natural U, suggesting that U in this sample may be a mixture of the end-member sources. Soil sample NTS 132 does not, suggesting that non-natural U in this sample may come from a different source.

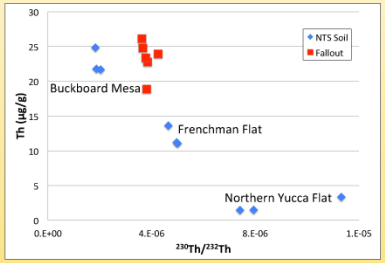

Soils collected from three different locations cluster with respect to location, as might be expected, suggesting Th isotopic composition is characteristic of rock type. Fallout shows less scatter relative to the soil values. This could be due to fallout formation mechanisms or the result of a uniform environmental contribution from a single location. Error bars are smaller than symbols.

Model "Age"

In the uranium decay series, ^{238}U decays to ^{234}U, which decays to ^{230}Th. By measuring the ratio of ^{234}U to ^{230}Th, a model age can be calculated, assuming no initial daughter (^{230}Th) and no addition or removal of ^{230}Th and ^{234}U after bead formation.

Using this method, we calculate model ages that varied from 163-213 years before present. These ages cannot be correct as above-ground testing was limited to the years 1945-1962. Thus, there is excess ^{230}Th relative to ^{234}U. To explain this, chemical fractionation between uranium and thorium may have occurred during the formation of the glassy fallout beads. It is unclear whether ^{230}Th was added or ^{234}U was lost during this process.

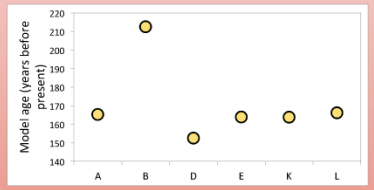

Conclusions

After performing the analyses we found that two of our soil samples contained non-natural uranium isotopic signatures. One looks like it was contaminated by a test with characteristics similar to the investigated glassy fallout beads, the other looks to be contamination of a entirely different composition.

Bulk analysis of the glassy beads showed, somewhat surprisingly, that they cluster in their isotopic compositions for uranium and thorium. Among the soils there are large variations in the thorium concentrations.

From these experiments we can deduce that when the fallout forms the HEU combines with the natural soil, creating a mixture of the two components which can be explained through a simple two component mixing model. There may be Th contributed from the device or during the formation of fallout glass Th and U are chemically fractionated from one another.

The fallout beads were all similar in their bulk isotopic compositions. Performing a simple correction for the environmental contributions making simple assumptions, we calculate a starting isotopic composition for the fallout of 92% ^{235}U, consistent with what might be expected. The correctness of our assumptions, however, cannot be verified with the present data.

LLNL-POST-XXXXXXX

This research was performed under the Nuclear Forensics Undergraduate Scholarship Program, which is sponsored by the U.S. Department of Homeland Security Domestic Nuclear Detection Office

This work performed under the auspices of the U.S. Department of Energy by Lawrence Livermore National Laboratory under Contract DE-AC52-07NA27344

Improved Geolocation of Uranium Ore Concentrate through Geochemical Insights

Erin Kenney[1], Martin Robel[2], Naomi Marks[2], Ian Hutcheon[2]
1. Massachusetts Institute of Technology
2. Lawrence Livermore National Laboratory, Chemical Sciences Division

Glenn T. Seaborg Institute

Abstract: Using the values of the rare earth element (REE) concentrations in UOC samples from six known sources, partial least squares discriminant analysis (PLS-DA) was performed in MATLAB to create a corresponding model of the data. Various preprocessing methods were applied to the data prior to the creation of the model, and the resulting success of the model in classifying unknown samples was gauged, according to the root-mean-square error of cross-validation (RMSECV). Preprocessing methods used include both geochemical and mathematical techniques, classified further as *basic, advanced, geochemical,* and *calculated geochemical ratios*. The lowest cross-validation error was achieved with a combination of geochemical and advanced general preprocessing techniques.

Introduction:

- The Uranium Sourcing Database contains trace element concentrations representing material from various uranium mines
- Total REE concentrations may vary substantially for material from a single mine, but the relative concentrations follow consistent patterns
- Geochemists use REE profiles to compare samples according to relative concentrations
- A classification experiment was performed using preprocessing based on geochemical methods
- Experiment included six different classes (known locations of origin) that each contained at least two samples: Niger, Portugal, Source C, Kazakhstan, Uzbekistan, and Yugoslavia
- REE concentrations and ratios were used as variables

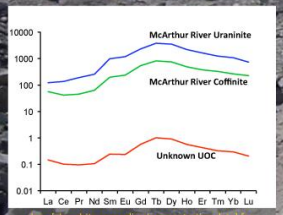

$\log_{10}$[chondrite-normalized concentration data] for McArthur River. Consistent shapes in REE profile plots indicate materials from the same source.

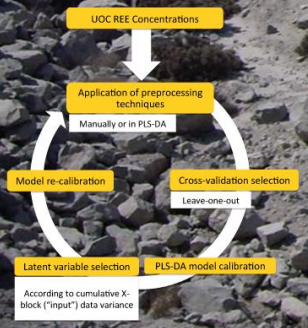

Data Preprocessing Experiment

Uranium Ore Concentrate Rare Earth Element Concentrations

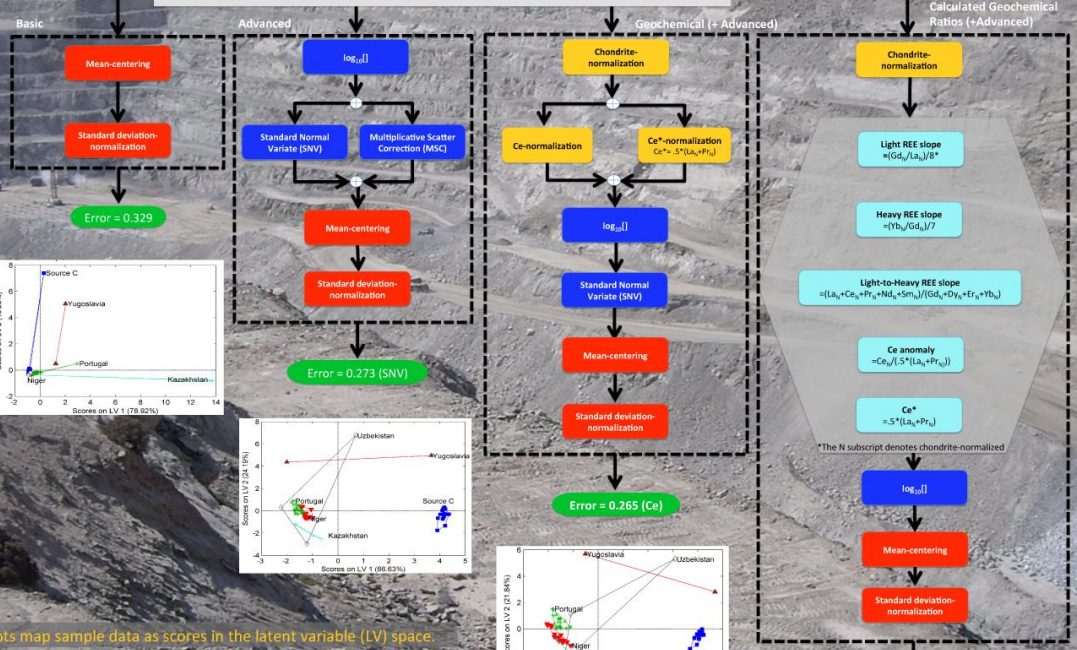

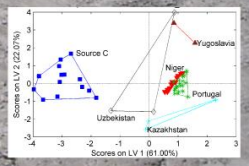

Plots map sample data as scores in the latent variable (LV) space.

Types of Preprocessing:

- Mean-centering: take REE (column) values minus the mean
- Standard deviation-normalization: divide REE values by respective REE's standard deviation
- MSC: compare data to a standard and adjust
- SNV: mean-centering and standard deviation-normalization of sample (row) values
- Ce-normalized: divide row by respective Ce concentration
- Ce*-normalized: divide row by respective Ce*, where Ce* = .5*(La_N+Pr_N)
- Chondrite-normalized: divide REE value by corresponding Anders and Grevesse (1989) normalization factor

Results:

- A PLS-DA model was tested for each preprocessing block (dashed boxes)
- The green boxes under each block show the error of leave-one-out cross-validation
- Preprocessing reduced the error by as much as 20%

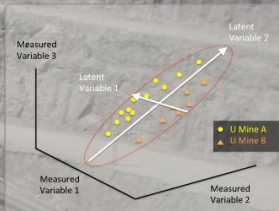

PLS-DA transforms measured data to fewer dimensions by rotating, scaling, and projecting for optimal discrimination. Measured variables in this study are trace rare earth element concentrations (parts per million).

Conclusions:

- Using *advanced* ($\log_{10}$[] and SNV) preprocessing reduced the classification error substantially by minimizing the influence of variable total impurity concentration
- Adding *geochemical* preprocessing techniques further reduced the classification error
- Using *calculated geochemical ratios* did not produce the lowest error, but could be more robust due to its underlying geochemical basis (as compared to a purely empirical model)

This work performed under the auspices of the U.S. Department of Energy by Lawrence Livermore National Laboratory under Contract DE-AC52-07NA27344.

Frozen in Time

Anna Lindquist[1], Kim Knight[2], Zurong Dai[2], Rick Ryerson[2], Ian Hutcheon[2], Greg Spriggs[2]
[1]University of Minnesota, Department of Earth Sciences, Minneapolis, MN
[2] Lawrence Livermore National Laboratory, Physical and Life Sciences, Chemical Sciences Division, Livermore, CA

Crystallinity and composition help to constrain the cooling environment of fallout.

Abstract

This poster looks at spheroidal glassy fallout beads from several near surface nuclear tests using transmission electron microscopy (TEM) and electron microprobe (EMP) analyses to investigate the crystallinity and distribution of elements within fallout. Fallout forms during near-surface nuclear tests as a result of superheated material rapidly cooling and falling to the ground. Preliminary studies (Gostic, 2011; Lindquist, 2011) have shown that most residual radioactivity is contained in glassy aerodynamic components which can be separated from fallout soils. These materials form within seconds after a detonation and often contain complicated major element and activity distributions. Our study characterizes compositional and structural variations to provide constraints on the environment and cloud conditions at the time of fallout formation. This continued work assists a more complete understanding of the conditions under which these materials form, thus aiding interpretation of the information preserved in these glasses.

Crystallinity

Transmission electron microscopy (TEM) creates images similarly to optical microscopy, but uses a beam of electrons instead of light. TEMs can collect information about morphology, structure, and chemical composition from very small (down to nanoscale) regions. In this study we used diffraction patterns, which illustrate the structure of the sample, and bright-field images, which show the morphology of a sample.

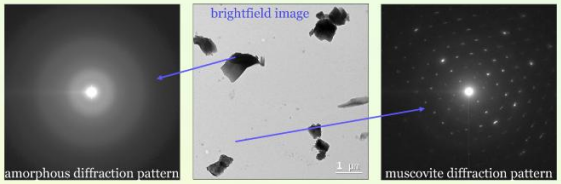

In the TEM, many of the fragments we found were glassy (above and below left). However, diffraction patterns showed that some regions were crystalline (above and below right).

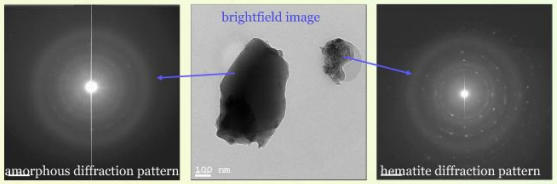

The presence of amorphous phases is expected because the material vaporized by a nuclear event undergoes rapid cooling. This means atoms may not have time to reform ordered structures.

Crystalline phases were observed in rare cases, but appear as distinct grains. Their diffraction patterns often match common rock forming minerals. A transition from disordered (amorphous) to more ordered (crystalline) phases was not observed within a single shard. The crystalline phases likely represent incompletely melted materials incorporated into the glassy spheres prior to quenching, rather than minerals crystallized from the silicate melt. Our sample preparation methods do not retain spatial information, so it is not possible to determine whether analyzed material originated from the interior or exterior of the bead.

This work performed under the auspices of the U.S. Department of Energy by Lawrence Livermore National Laboratory under Contract DE-AC52-07NA27344

Composition

Electron microprobe (EMP) analysis was used to collect compositional data from polished glassy fallout beads. An EMP uses a beam of electrons to excite atoms from the sample surface. As the atoms return to lower energy states, X-rays with characteristic wavelengths are emitted and detected by the EMP to determine the composition of the sample.

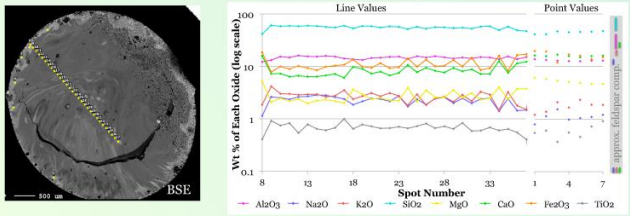

We collected qualitative compositional maps (below) and quantitative spot analyses (above). In the backscattered electron (BSE) image above bright areas represent higher average atomic number, and darker areas lower average atomic number. Yellow spots indicate quantitative EMP spot analyses and correlate to the graph (above right). This bead is fairly typical of the average composition and compositional variation within the fallout beads we studied. Composition data can be used to approximate the solidification temperature via known oxide melting points.

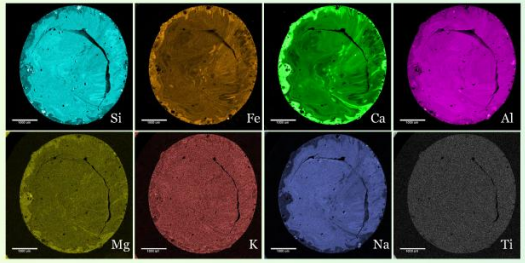

EMP maps (above) show the distribution of select major elements. Some elements tend to concentrate in different regions of the bead, such as enrichment of Ca and Fe in the rim. Swirled, mixing-like patterns of element variation are a common feature in these beads. Electron imaging shows little evidence for the presence of discrete mineral grains within beads, though relic or partially melted grains (based on sharp compositional boundaries and 2-D morphology) may be present in rare cases.

Fallout Samples and Sample Preparation

These two fallout beads (below left and center) illustrate the type of samples used for this study and some of the variety of morphologies observed. Crushed fragments from beads like these were deposited on copper grids (below right) for TEM work. Whole beads were embedded in resin and polished for EMP work.11

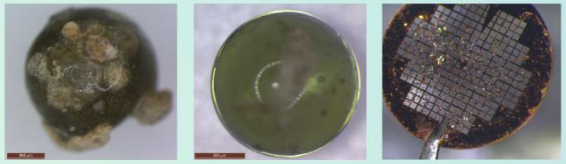

Cooling Environment

Conclusions

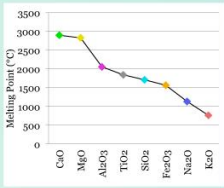

- The fireball from a 0.01–100 Kt weapon cools to ~2500°C within seconds (Spriggs, 2011).
- Temperatures at which oxide species transition from liquid to solid (right) can be used to understand the cooling regime of fallout.
- Most bead material is amorphous, suggesting very rapid quenching of the silicate liquid.
- Glassy material is feldspathic in composition, consistent with the dominant source material for the silicate melts being surrounding dirt and soil (Jacomb-Hood, 2012).

- Crystalline regions are observed, but generally as discrete phases, separated from the bulk of the matrix.
- Crystalline diffraction patterns often match common rock-forming mineral phases.
- Crystalline materials are likely included grains from the dust and debris of the surrounding environment, not phases that crystallized during quenching of the silicate melts or unmelted device components.

References

1) Gostic, Richard et al. (2011), LLNL-POST-492931.
2) Jacomb-Hood, Timothy et al. (2012), LLNL-POST-570154
3) Lindquist, Anna et al. (2011), Feelin', hot, hot, hot!, LLNL-POST-492773.
4) Spriggs (2011), Thermal pulses from a nuclear detonation, LLNL-PRES-468671.
5) webelements.com, accessed July 31, 2012.

LLNL-POST-569061

Nuclear Forensics Signatures in Uranium Bearing Materials

LA Meyers[1,2], RW Williams[2], SE Glover[1], SP Lamont[3], AM Stalcup[1], HB Spitz[1]

1. University of Cincinnati, Cincinnati, OH 45221

2. Lawrence Livermore National Laboratory, PLS, Chemical Science Division, Livermore, CA 94550

3. Department of Energy, Washington DC, 20585

Glenn T. Seaborg Institute

UNIVERSITY OF Cincinnati

Introduction

Nuclear forensics is a multidisciplinary science that uses a variety of analytical methods and tools to explore the physical, chemical, elemental, and isotopic characteristics of nuclear and radiological material. These signatures may allow determination of the materials provenance and the method of manufacture. The uranium isotopic composition reveals whether the uranium is natural, depleted, or enriched and whether the material has ever been subjected to neutron irradiation and subsequently reprocessed. The radiochronology (*i.e.*, age dating) presented here determines the time since purification of a uranium-bearing material based upon the ingrowth of ^{230}Th toward its parent ^{234}U in a non-disturbed environment. The uranium decay series and the position of ^{230}Th and ^{234}U in the sequence of decay products is shown in **Figure 1**. In this work, a variety of uranium bearing materials are analyzed to determine the nuclear forensic signatures in each sample.

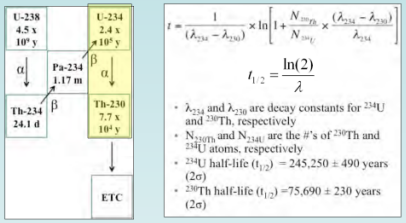

$$t = \frac{1}{(\lambda_{234} - \lambda_{230})} \times \ln\left[1 + \frac{N_{^{230}Th}}{N_{^{234}U}} \times \frac{(\lambda_{234} - \lambda_{230})}{\lambda_{234}}\right]$$

$$t_{1/2} = \frac{\ln(2)}{\lambda}$$

- λ_{234} and λ_{230} are decay constants for ^{234}U and ^{230}Th, respectively
- $N_{^{230}Th}$ and $N_{^{234}U}$ are the #'s of ^{230}Th and ^{234}U atoms, respectively
- ^{234}U half-life ($t_{1/2}$) = 245,250 ± 490 years (2σ)
- ^{230}Th half-life ($t_{1/2}$) =75,690 ± 230 years (2σ)

Figure 1: ^{238}U decay chain displaying the decay of ^{234}U to ^{230}Th, on the left, and the equation to determine the age of young uranium samples, on the right. Half-lives from [1].

Experimental

Sample Preparation:

- The uranium metal samples were digested with nitric acid. The soil samples were digested with nitric and hydrofluoric acid. Sample aliquots were spiked with ^{233}U, ^{229}Th, or ^{244}Pu and processed through several separation and purification steps shown in **Figure 2**.

Instrumentation:

- Samples were analyzed using the following type of instrumentation:
  - •MC-ICP-MS
  - •SEM/EDS
  - •Quad-ICP-MS

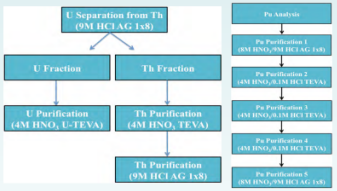

Figure 2: The U and Th separation scheme for soil and metal samples (for Th analysis only on metal samples) is shown on the left, and the Pu separation scheme is shown on the right.

This work performed under the auspices of the U.S. Department of Energy by Lawrence Livermore National Laboratory under Contract DE-AC52-07NA27344.

Nuclear Forensics Scenario

Samples analyzed from an abandoned metal rolling facility are shown in the pictures below. The U metal was found in the raw soil that was collected from the facility. [2]

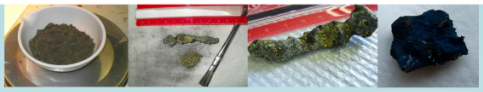

Raw Soil U Metal Dust U Metal Scrapings U Metal

The uranium isotopic composition of the uranium metal and soil samples, shown in **Table 1** and **Figure 3**, match that of natural uranium. The total uranium concentrations for each sample are also shown in **Table 1**.

Sample description	^{238}U, atom %	^{236}U, atom %	^{235}U, atom%	^{234}U, atom%	U, g/g
U Metal Scrapings	99.27 ± 0.12	None detected[a]	0.7206 ± 0.0006	0.005414 ± 1.7·10^{-5}	0.586 ± 0.011
U Metal Dust	99.27 ± 0.12	1.68·10^{-6}± 5.3·10^{-7}	0.7200 ± 0.0006	0.005409 ± 1.7·10^{-5}	0.257 ± 0.005
Raw Soil	99.28 ± 0.12	2.33·10^{-6}± 5.5·10^{-7}	0.7176 ± 0.0006	0.005382 ± 1.7·10^{-5}	0.048 ± 0.001
U Metal #1	99.27 ± 0.14	None detected[a]	0.7200 ± 0.0013	0.005420 ± 1.7·10^{-5}	0.984 ± 0.005
U Metal #2	99.27 ± 0.14	None detected[a]	0.7205 ± 0.0013	0.005410 ± 1.7·10^{-5}	0.886 ± 0.008
U Metal #3	99.27 ± 0.14	None detected[a]	0.7206 ± 0.0013	0.005414 ± 1.7·10^{-5}	0.900 ± 0.008
Natural Uranium[3]	99.27 ± 0.0015	0	0.7200 ± 0.0012	0.005500 ± 0.0055	

* U uncertainties are given as the combined standard uncertainty.
a ^{236}U was determined to contribute less than 1e-6 atom percent based on the detection limit.

Table 1. Uranium isotopic composition and uranium concentrations for each sample. [3]

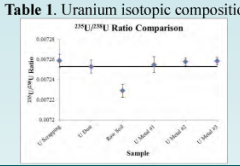

Figure 3. ^{235}U/^{238}U ratio comparison between the soil and U metal samples. All samples resemble that of natural uranium (solid black line) except for the raw soil sample, which has a slightly depleted uranium signature. (Error bars show combined standard uncertainty (k=1)).

Comparison of Uranium Metals

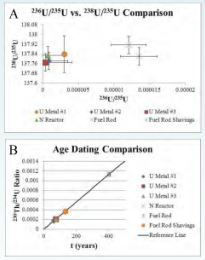

Figure 4. A.) Uranium ratio comparison plot for each metal sample. (Error bars represent k=1) B.) Age dating comparison for each metal sample. (Error bars represent k=3).

Sample description	U, g/g
U Metal #1	0.984 ± 0.005
U Metal #2	0.886 ± 0.008
U Metal #3	0.900 ± 0.008
N Reactor	1.003 ± 0.009
Fuel Rod	0.929 ± 0.007
Fuel Rod Shavings	0.932 ± 0.008

* U uncertainties are given as the combined standard uncertainty.

Table 2. Uranium concentrations for each metal sample.

Four uranium metal samples were analyzed for nuclear forensic signatures. The fuel rod and fuel rod shaving samples have a significant amount of ^{236}U and the model ages are older than their expected age. The ^{236}U signature indicates that these samples may contain a component of recycled irradiated uranium. The model age of the metal samples appears older than the expected age due to excess initial ^{230}Th. [4]

Comparison of Metal Rolling Facility Soils

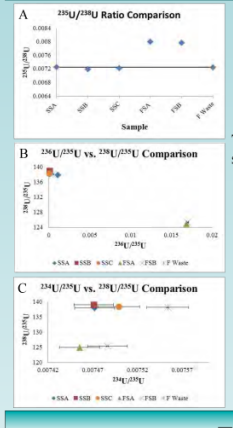

Sample description	U, g/g	Pu, pg/g
SSA	0.0215 ± 1.02·10^{-4}	0.067 ± 0.022
SSB	0.0393 ± 2.48·10^{-4}	0.057 ± 0.021
SSC	0.0486 ± 9.61·10^{-4}	Not Analyzed
FSA	0.0021 ± 9.67·10^{-6}	141.5 ± 1.7
FSB	0.0018 ± 7.78·10^{-6}	137.4 ± 1.8
F Waste	0.0027 ± 1.44·10^{-5}	None detected

* U uncertainties are given as the combined standard uncertainty.

Table 3. Uranium and plutonium concentrations of each soil sample.

Two metal rolling facilities are distinguished from one another through analysis soil samples from each facility and comparison of their nuclear forensic signatures. Soil samples FSA and FSB have slightly enriched uranium signatures as well as a significant ^{236}U content compared to the SSA-SSC soils. Soil samples SSA-SSC have a higher uranium content, and soil samples FSA-FSB have higher Pu concentrations.

Figure 5. A.) ^{235}U/^{238}U ratio comparison of soil samples. B and C.) Minor uranium isotope comparison plots of soil samples. (Error bars are k=1 in all plots)

Future Work

•Analysis of uranium ore samples for signatures:

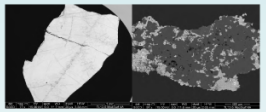

Pitchblende Ore US Western Ore

•Analyze ore and metal samples for REE signatures:

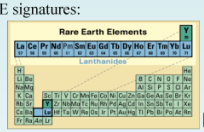

[5]

Conclusions

- Analyzing both uranium metal and soil samples from a metal rolling facility for nuclear forensic signatures can tell two sides of a story.
  1.) The history of the U metal itself, and 2.) Indicate other work that was done at the facility.
- The uranium metal is better suited for forensic analysis, as it may be a closed-system.
- Soil samples are mixtures of natural (old), and anthropogenic (young) material.
- Radiochronometry is an important tool in determining the provenance of nuclear or radiological material, but has its limitations.

References

[1] Cheng H, Edwards RL, Hoff J, et al (2000) Chem Geol 169:17-33
[2] Meyers LA, Williams RW, et al (2012) J Radioanal Nucl Chem (accepted)
[3] Browne E, Firestone RB, Shirley VS (1986) Table of Radioactive Isotopes. John Wiley & Sons, Inc., New York
[4] McCulloch MT, Mortimer GE (2008) Aust J Earth Sci 55: 955-965
[5] http://pubs.usgs.gov/fs/2002/fs087-02/

First Principles Study of $AnO_2(NO_3)_2(H_2O)_2$ (An=U, Pu) VI to V Reduction Potential

[2]Mitchell Goshert, [1]Patrick Huang, and [2]Justin Walensky

Physical and Life Sciences Directorate and Glenn T. Seaborg Institute

[1]Lawrence Livermore National Laboratory

[2]University of Missouri

INTRODUCTION

- Aqueous uranyl and plutonyl dinitrates are common by-products of nuclear fuel reprocessing.
- What is their long-term mobility and fate?
- Oxidation state determines solubility and consequently the mobility in the environment.
- What are the thermodynamic parameters characterizing the transformation between oxidation states?
- Actinides in solution exhibit a large variation in oxidation state and coordination number.
- Contributions due to variations in actinide speciation difficult to disentangle experimentally.
- Calculations of reduction potential can provide useful insight on the energy required to reduce these actinide species.

THEORETICAL METHODOLOGY

Hartree-Fock (HF)

$$\left[-\frac{\hbar^2}{2m}\nabla_i^2 + V_i^{\text{eff}}(\mathbf{r}_i)\right]\varphi_i(\mathbf{r}_i) = \varepsilon_i\varphi_i(\mathbf{r}_i)$$

- Mean field approximation: Each electron feels the same averaged, effective potential due to the remaining electrons.
- Does not include electron-electron correlation → qualitative, but not quantitatively accurate.
- Useful as starting point for higher-level theories.

Density Functional Theory (DFT)

- Mean-field theory (like Hartree-Fock)
- Approximate inclusion of electron correlation via model exchange-correlation functional v_{xc}.
- We employ the B3LYP approximation for v_{xc}:
  1. Generally improves bond energies and lengths over HF,
  2. Better-suited for localized d- or f-electrons (minimizes self-interaction error)

SOLVENT MODEL

Conductor-like Polarizable Continuum Model (CPCM)

- Solvent effects are an important influence on reduction potentials.
- Model solvent as a continuum dielectric.
- Need to assume a conductor-like cavity containing solute.
- CPCM well-established for polar solvents (e.g., water).

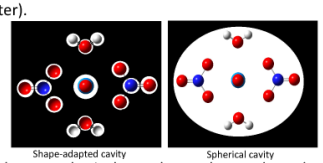

Shape-adapted cavity | Spherical cavity

- For large, aspherical complexes, shape-adapted cavities are necessary.

CALCULATION OF REDUCTION POTENTIALS

- Free energies are calculated relative to a standard hydrogen electrode.
- ΔG for each half-reaction is calculated separately, then summed to obtain the overall process.

$$An^{VI} + e^- \rightarrow An^{V}$$

$$\frac{1}{2}H_2 + H_2O \rightarrow H_3O + e^-$$

$$An^{VI} + \frac{1}{2}H_2 + H_2O \rightarrow An^{V} + H_3O$$

OPTIMIZATION OF BOTH U(VI) AND U(V) SPECIES

- Both the HF and the DFT-B3LYP level of theory were employed.
- The structures of the $UO_2(NO_3)_2(H_2O)_2$ complex in both U (VI) and U(V) oxidation states were optimized.
- Vibrational analysis was employed to verify the stability of optimized structures.

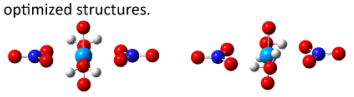

- The optimized structures of U(VI) (left) and U(V) (right)

STRUCTURES

$U^{VI}O_2(NO_3)_2(H_2O)_2$ – Bond Lengths

		HF (gas)	B3LYP (gas)	B3LYP (solv)	Expt.
U=O	[Å]	1.71	1.77	1.77	1.76
$U\text{-}O_{H2O}$	[Å]	2.56	2.55	2.52	2.45
$U\text{-}O_{NO3}$	[Å]	2.50	2.49	2.50	2.48

*Experimental data from Dalley, N.K.; Mueller, M.H.; Simonsen, S.H *Inorganic Chemistry* Vol. 10, No.2, 323 (1971).

- HF theory yields significant lengthening of both bonds relative to experiment.
- B3LYP shows an improved U=O bond length to within ~ 0.01 Å.
- The $U\text{-}O_{H2O}$ is significantly lengthened at both levels of theory.
- Both HF and B3LYP accurately predict the $U\text{-}O_{NO3}$ bond length within ~0.02 Å.

$U^{V}O_2(NO_3)_2(H_2O)_2$ – Bond Lengths

		HF (gas)	B3LYP (gas)	B3LYP (solv)	Expt.
U=O	[Å]	-	1.84	1.85	-
$U\text{-}O_{H2O}$	[Å]	-	2.71	2.62	-
$U\text{-}O_{NO3}$	[Å]	-	2.61	2.61	-

- Uranyl V bond lengths show ~0.1 Å increase on average over uranyl VI.
- This is expected due to the additional electron decreasing the effective nuclear charge, consequently decreasing the U-O attraction and increasing the bond lengths.

FREQUENCIES

$U^{VI}O_2(NO_3)_2(H_2O)_2$ - Frequencies

U=O		HF (gas)	B3LYP (gas)	B3LYP (solv)
v_s	[cm^{-1}]	1062.0	894.5	880.9
v_{as}	[cm^{-1}]	1119.6	979.6	943.2

- HF yields shorter, stiffer bonds
- Inclusion of solvent slightly red-shifts frequencies

$U^{V}O_2(NO_3)_2(H_2O)_2$ – Frequencies

U=O		HF (gas)	B3LYP (gas)	B3LYP (solv)
v_s	[cm^{-1}]	-	800.6	785.1
v_{as}	[cm^{-1}]	-	852.0	795.3

- Uranyl V frequencies are greatly red-shifted compared to uranyl VI,
- This is expected due to the increase in bond lengths

REDUCTION POTENTIALS

		ΔG (gas)	ΔG (solv)
U(VI) + e^- -> U(V)	[eV]	2.86	4.60
$½H_2 + H_2O$ -> $H_3O^+ + e^-$	[eV]	-8.96	-5.78
Reduction Potentials	[eV]	-6.10	-1.18

- Inclusion of solvation effects yields a ~ 4.9 eV improvement over the gas phase model.
- Discrepancy between ΔG (solv) and expt likely due to:
  1. Errors in H2 half-reaction.
  2. Lack of explicit second coordination sphere.
- Errors for calculated actinide reduction potential typically ~ 2-3 eV [Hay, J. P.; Martin, R. L.; Schreckenbach, G. J. Phys. Chem. A 2000, 104]
- Experimental data for the reduction potential of $UO_2(H_2O)_5$ is 0.16 eV, meaning our data is reasonable [Brand, J. R.; Cobble, J. W. *Inorg. Chem.* 1970 , 9, 912.]

CONCLUSIONS

- Benchmark studies have been done on the $UO_2(NO_3)_2(H_2O)_2$ VI and V compounds.
- Our model involves an explicit representation of the first coordination sphere plus a continuum dielectric for the solvent environment.
- Solvation effects are essential for description of reduction potentials.

FUTURE WORK

- Secondary coordination sphere in the solvent model still need to be included for further improvement in reduction potential values
- Spin-orbit correction
- Improved treatment of electron correlation (second order perturbation theory, MP2)
- Plutonyl calculations

ACKNOWLEDGEMENTS

- M.G. gratefully thanks the Glenn T. Seaborg Institute for their financial support.

This work performed under the auspices of the U.S. Department of Energy by Lawrence Livermore National Laboratory under Contract DE-AC52-07NA27344.

Cosmogenic Activation in the Neutrinoless Double-beta Decay Experiment CUORE

Barbara S. Wang[1], Eric B. Norman[1], Nicholas D. Scielzo[2], Marisa Pedretti[2], Stephen A. Wender[3], Alan R. Smith[4], Keenan J. Thomas[1,4], Yuen-dat Chan[4]

[1]University of California, Berkeley; [2]Lawrence Livermore National Laboratory; [3]Los Alamos National Laboratory; [4]Lawrence Berkeley National Laboratory

Abstract: CUORE (Cryogenic Underground Observatory for Rare Events) is an experiment that will search for neutrinoless double-beta (0νββ) decay. The CUORE detector is an array of 988 high-resolution, low-background TeO_2 bolometers operated at cryogenic temperatures. All sources of background that can obscure the 0νββ decay signature must be well-understood. One of these sources is cosmogenic activation of the bolometers. A reliable estimation of this background is essential but difficult to obtain because of the lack of cross-section data. Thus, cross-section measurements have been carried out at LANSCE (Los Alamos Neutron Science Center).

Introduction

Double-beta Decay

2νββ: $(A,Z) \rightarrow (A,Z+2) + 2e^- + 2\bar{\nu}_e$

Allowed by Standard Model

0νββ: $(A,Z) \rightarrow (A,Z+2) + 2e^-$

Not allowed by Standard Model

- Physics questions to answer:
  - Is ν Majorana or Dirac particle?
  - What is neutrino mass scale and hierarchy?
  - Is lepton number conserved?

CUORE Detector

- Located underground at Gran Sasso National Laboratory in Italy
- Data-taking starts 2015
- 988 TeO_2 bolometers at 10 mK (natural Te used)
- 0νββ decay reaction: $^{130}Te \rightarrow {}^{130}Xe + 2e^-$ (Decay energy = 2527 keV. Isotopic abundance of ^{130}Te = 34%)

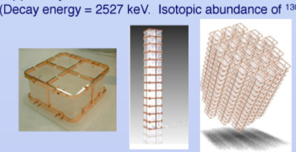

Bolometer Mechanics

- Interaction in TeO_2 crystal
- Temperature rise (ΔT) measured
- Energy deposition in crystal derived from E=CΔT (C = heat capacity)

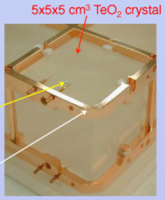

Double-beta Decay Signatures in CUORE

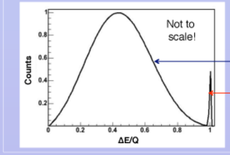

- ΔE = energy deposition in detector
- Q = decay energy
- 2νββ decay signature: energy continuum up to Q
- 0νββ decay signature: peak at Q (2527 keV for CUORE)

Background Events

- An event that is not 0νββ decay and can obscure the 0νββ decay peak is considered background
- Need extremely low background in region around 2527 keV (gray in the figure)
- CUORE's goal background at 2527 keV: 0.001 – 0.01 counts/keV/kg/year
- All sources of background must be well-understood

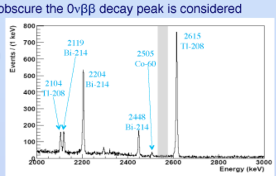

- Background due to cosmogenic activation of the TeO_2 bolometers highly uncharacterized

Cosmogenic Activation in CUORE

- **Cosmogenic activation: Interactions with cosmic rays produce radioisotopes in materials.**
  - Occurs during transportation
  - Each crystal spends ~ 4 months above ground at sea-level
  - Long-lived radioisotopes produced in TeO_2 contribute background at 0νββ decay peak

Example: Beta decay of Co-60 ($t_{1/2}$ = 5.27 y)

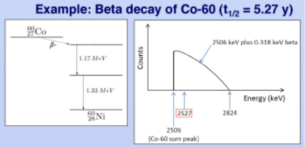

Methods and Results

At sea-level, most cosmogenic activation due to interactions with cosmic ray neutrons.

Cross-section measurements have been performed at LANSCE for neutron activation of radioisotopes in TeO_2

LANSCE (Los Alamos Neutron Science Center)

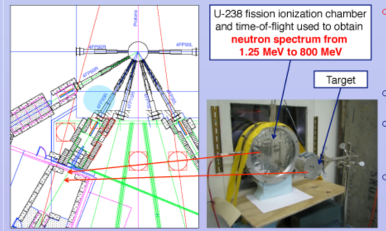

- 0-800 MeV neutrons produced by spallation of 800 MeV protons on tungsten
- Proton beam is pulsed
- Neutron energies obtained from time-of-flight data.
- Flux-shape of neutrons along 30°-right flight path similar to that of cosmic ray neutrons at sea-level

Methods and Results (cont.)

LANSCE Neutron Spectrum

(compared with cosmic ray neutron spectrum at sea-level)

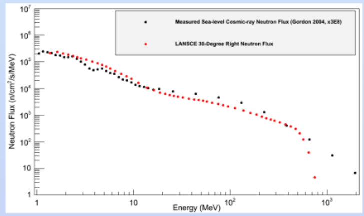

Cross-section Measurement Information

- Target:
  - 272 g TeO_2 powder
  - Al and Au foils (monitor neutron flux)
  - Cd foil (remove thermal neutrons)
- Target diameter: 6.4 cm
- Beam diameter at target: 8.4 cm
- Neutron flux at target: 1.4E6 n/cm²/s
- Irradiation time: 42 h

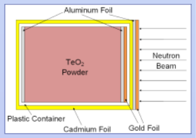

Gamma Measurement Following Irradiation

- TeO_2 powder thoroughly mixed and placed in Marinelli beaker
- Powder counted periodically for 4 months with HPGe detector

(Photo taken from: http://www.ga-maassociates.com)

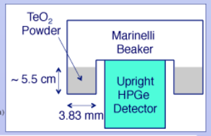

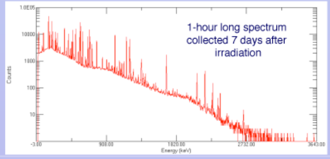

Radioisotopes Present in TeO_2	Half-life
Te-118	6.00 d
Te-119m	4.7 d
Te-121	19.17 d
Te-121m	164.2 d
Te-123m	119.2 d
Te-125m	57.4 d
Te-127	9.35 h
Te-127m	106.1 d
Te-129	69.6 m
Te-129m	33.6 d
Te-131	25 m
Te-131m	33.25 h
Xe-131m	11.84 d
Sb-118	3.6 m
Sb-119	38.19 h
Sb-120m	5.76 d
Sb-122	2.7238 d
Sb-124	60.2 d
Sb-125	2.75856 y

Radioisotopes Present in TeO_2	Half-life
Sb-126	12.35 d
Sb-127	3.85 d
Sn-113	115.09 d
Sn-117m	14 d
Sn-123	129.2 d
Sn-125	9.64 d
Rh-100	20.8 h
Rh-101m	4.34 d
In-111	2.8047 d
In-114m	49.51 d
I-126	12.93 d
I-131	8.0252 d
Cd-115	53.46 h
Ag-105	41.29 d
Ag-106m	8.28 d
Ag-110	24.6 s
Ag-110m	249.76 d
Ag-111	7.45 d
Be-7	53.24 d

Isotopes in yellow can contribute to 0νββ decay region (around 2527 keV peak)

Cross-section Calculations

- Using peaks in the gamma spectrum, a flux-averaged cross-section (σ) was obtained for each isotope seen in TeO_2.

$\sigma_i(E)$ = Production cross-section for isotope i [cm²]

$\varphi_{LANSCE}(E)$ = LANSCE neutron spectrum [n/MeV/cm²/s]

(Only includes neutrons with energies 1.25-800 MeV)

$$\bar{\sigma}_i = \frac{\int \sigma_i(E)\varphi_{LANSCE}(E)dE}{\int \varphi_{LANSCE}(E)dE}$$

- To obtain σ, the absolute peak efficiency must be known.
- Absolute peak efficiency measurement:
  - A source with the same density and geometry as the TeO_2 powder was created using a powder mixture and a Marinelli beaker.
  - Composition of powder mixture:

Compound	Mass (g)	Activity (Bq)
TeO_2 powder	228	0
Lu_2O_3 powder	6	278
La_2O_3 powder	23	17
K_2SO_4 powder	14	194
Total	271	489

  - Mixture was counted with the same HPGe detector used to count TeO_2 powder.
  - The absolute peak efficiency as a function of gamma-energy was obtained.
  - Summing effects due to the radioactive isotopes in the TeO_2 powder need to be included. These are currently being obtained using Monte Carlo simulations.
- Preliminary cross-sections for two most important isotopes seen in TeO_2:

Radioisotope	Half-life (d)	Cross-section (mb)	+/- (mb)
Ag-110m	249.8	0.17	0.02
Sb-124	60.2	12.7	1.7

Both of these isotopes have long half-lives and can contribute to 0νββ decay region.

Current and Future Work:

- Currently using Ag-110m and Sb-124 cross-sections in a Monte Carlo simulation of the entire CUORE detector to estimate the cosmogenic activation background that will be present in CUORE

Supported by the U.S. Dept of Energy, Office of Defense Nuclear Nonproliferation (NA-22), LLNL under Contract DE-AC52-07NA27344, and a Nuclear Forensics Graduate Fellowship from the U.S. Dept of Homeland Security, DNDO and the U.S. Dept of Defense, DTRA.

IM Release Number: LLNL-POST-569453

This work was performed under the auspices of the U.S. Department of Energy by Lawrence Livermore National Laboratory under Contract DE-AC52-07NA27344.